

Neutron-diffraction study of the magnetic ordering in EuAs_3 , $\text{Eu}(\text{As}_{1-x}\text{P}_x)_3$, and $\beta\text{-EuP}_3$

T. Chattopadhyay

Centre d'Etudes Nucléaires, Département de Recherche Fondamentale, Service de Physique-Group Magnétisme et Diffraction Neutronique, 85X, 38041 Grenoble Cedex, France

P. J. Brown

Institute Laue-Langevin, 156X, 38042 Grenoble Cedex, France

P. Thalmeier

Institut für Theoretische Physik, Rheinisch-Westfälische Technische Hochschule, D-5100 Aachen, Federal Republic of Germany

W. Bauhofer and H. G. von Schnering

Max-Planck-Institut für Festkörperforschung, Heisenbergstrasse 1, D-7000 Stuttgart 80, Federal Republic of Germany

(Received 4 May 1987)

Magnetic ordering in EuAs_3 , $\text{Eu}(\text{As}_{1-x}\text{P}_x)_3$, and $\beta\text{-EuP}_3$ has been determined by neutron diffraction on single crystals. Semimetallic EuAs_3 and $\text{Eu}(\text{As}_{1-x}\text{P}_x)_3$ with $x \leq 0.98$ order at T_N (11.4–8.5 K), with a second-order phase transition to a sine-wave amplitude modulated phase with the magnetic moment $\mathbf{m} \parallel [010]$ or $[0\bar{1}0]$ direction. As the temperature is lowered these compounds undergo a further first-order phase transition at T_L (10.3–7.5 K), either to a commensurate antiferromagnetic phase with $\mathbf{m} \parallel [010]$ or $[0\bar{1}0]$ for lower P concentrations, or to a helimagnetic phase with magnetic moments modulated in direction and amplitude in the (010) plane for higher P concentrations. The semiconducting $\beta\text{-EuP}_3$, on the other hand, is a simple antiferromagnet with a second-order phase transition at $T_N = 10$ K, which shows no further temperature-induced phase transition down to $T = 2$ K. The condition for the existence of the incommensurate EuAs_3 has been investigated phenomenologically by varying the exchange interactions. A simple interpretation of the smooth temperature dependence of the modulation vector of the incommensurate EuAs_3 is given in terms of the sine-Gordon soliton-lattice model.

I. INTRODUCTION

Europium triarsenide EuAs_3 , europium triphosphide EuP_3 , and their solid solutions $\text{Eu}(\text{As}_{1-x}\text{P}_x)_3$ form an interesting system with varied electrical and magnetic properties^{1–8} (crystallographic data, electrical, and magnetic properties are given in Tables I and II). EuAs_3 is semimetallic, whereas EuP_3 has semiconducting properties.³ The solid solutions $\text{Eu}(\text{As}_{1-x}\text{P}_x)_3$ are semimetallic for $x \leq 0.98$. The charge-carrier density decreases as the concentration x of phosphorus atoms increases. These compounds consist of Eu^{2+} ions and two-dimensional infinite-layer puckered polyanions with a net effective charge of $2-$ per three X atoms, labeled ${}_{\infty}^2[X_3^{2-}]$, formed by phosphorus and/or arsenic atoms.¹ Eu^{2+} ions are in a ${}^8S_{7/2}$ ground state and have no orbital moment. Specific heat, susceptibility, and electrical-resistivity measurements³ suggest that EuAs_3 undergoes two successive phase transitions at 11.3 and 10.4 K. Recent neutron-diffraction experiments^{4,5} have established that EuAs_3 undergoes a second-order phase transition at T_N to an incommensurate antiferromagnetic phase with a propagation vector $(-1, 0, q_m)$ in which q_m is strongly temperature dependent. At $T_L = 10.3$ K this in-

commensurate phase undergoes a lock-in transition to a commensurate antiferromagnetic phase with the wave vector $(-1, 0, \frac{1}{2})$. EuAs_3 also shows four magnetic-field-induced phases^{6,7} when the external magnetic field is applied along the $[010]$ direction. On the other hand, specific-heat, susceptibility, and electrical-resistivity experiments³ show that the semiconducting $\beta\text{-EuP}_3$ orders in a single step at 10 K. Magnetization experiments⁷ show that $\beta\text{-EuP}_3$ has the classical spin-flop behavior in a single step. However, $\text{Eu}(\text{As}_{1-x}\text{P}_x)_3$ undergoes two-step magnetic ordering and has a complicated magnetic (H, T) phase diagram up to $x \leq 0.98$. Obviously, the two-step magnetic ordering behavior and the existence of several magnetic-field-induced transitions are directly related to the charge-carrier density and the resulting effective magnetic interactions of semimetallic EuAs_3 and $\text{Eu}(\text{As}_{1-x}\text{P}_x)_3$ with $x \leq 0.98$. The existence of the incommensurate intermediate phase and the lock-in transition to a commensurate phase can only be understood in terms of competing anisotropic magnetic interactions.⁵ The microscopic origin of this anisotropy is not yet understood. We have therefore undertaken systematic neutron-diffraction investigations of EuAs_3 , $\beta\text{-EuP}_3$, and $\text{Eu}(\text{As}_{1-x}\text{P}_x)_3$ to determine the magnetic or-

TABLE I. Crystallographic data of EuAs_3 , $\text{Eu}(\text{As}_{1-x}\text{P}_x)_3$, and $\beta\text{-EuP}_3$. The space group for all compounds is $C2/m$.

| Compound | T (K) | a (Å) | b (Å) | c (Å) | β (deg) | Z | V for $Z=4$ (Å ³) | Struct. type | Ref. |
|--|---------|-----------|--------------------|----------|---------------|-----|---------------------------------|-----------------|-----------|
| EuAs_3 | 295 | 9.471(2) | 7.598(2) | 5.778(2) | 112.53(5) | 4 | 384.1 | BaAs_3 | 1,8 |
| $\text{Eu}(\text{As}_{0.60}\text{P}_{0.40})_3$ | 295 | | | | | 4 | | BaAs_3 | |
| $\text{Eu}(\text{As}_{0.02}\text{P}_{0.98})_3$ | 295 | 9.068(1) | 7.222(1) | 5.998(1) | 113.15(3) | 4 | 336.2 | BaAs_3 | 8 |
| $\beta\text{-EuP}_3$ | 295 | 11.307(3) | 7.345(2) | 8.453(2) | 103.39(3) | 8 | 340.5 | SrP_3 | 8 |
| EuAs_3 | 5 | 9.43(2) | 7.50(1) | 5.75(1) | 112.48(5) | 4 | 375.6 | BaAs_3 | this work |
| $\text{Eu}(\text{As}_{0.60}\text{P}_{0.40})_3$ | 10 | 9.294(3) | 7.222 ^a | 5.691(2) | 112.79(1) | 4 | 352.2 | BaAs_3 | this work |
| $\text{Eu}(\text{As}_{0.02}\text{P}_{0.98})_3$ | 4.2 | 9.059(5) | 7.222 ^a | 5.576(1) | 113.15(3) | 4 | 335.4 | BaAs_3 | this work |
| $\beta\text{-EuP}_3$ | 5 | 11.23(1) | 7.345 ^a | 8.394(9) | 103.34(4) | 8 | 336.8 | SrP_3 | this work |

^a b values were not refined because of the lack of centered reflection with higher k values.

dering and to attempt to understand its origin.

The present paper is organized in the following way: Section II is devoted to the experimental details, and Secs. III–VI describe the results of neutron-diffraction experiments on the magnetic ordering in EuAs_3 , $(\text{EuAs}_{0.60}\text{P}_{0.40})_3$, $(\text{EuAs}_{0.02}\text{P}_{0.98})_3$, and $\beta\text{-EuP}_3$. In Sec. VII we propose a model for the origin of the first magnetic phase at T_N in EuAs_3 . In Sec. VIII we discuss the lock-in transition (sine wave to commensurate) in the context of sine-Gordon soliton-lattice theory. The sine wave to helimagnetic transition is also qualitatively discussed by using group-theoretical and energetic arguments. Finally in Sec. IX we give the summary and main conclusions from the present investigations.

II. EXPERIMENTAL PROCEDURE

EuAs_3 , EuP_3 , and $\text{Eu}(\text{As}_{1-x}\text{P}_x)_3$ were synthesized from the elements using Eu of 99.9% purity and As and P of 99.999% purity as starting materials.^{1,3} Large single crystals were grown by the Bridgman technique. The composition x of $\text{Eu}(\text{As}_{1-x}\text{P}_x)_3$ was determined by atomic emission spectroscopy with an accuracy of $\pm 1\%$. The crystallographic orientations of the crystals were determined by backreflection x-ray Laue photographs. The crystals were then cut to a desired size by a diamond saw.

Neutron-diffraction measurements were performed using the D15 diffractometer at the high-flux reactor of the Institut-Laue-Langevin in Grenoble. The diffractometer

was used in normal beam geometry at a wavelength $\lambda = 1.174$ Å. A single crystal of EuAs_3 of size $1 \times 1 \times 5$ mm³ with the largest dimension parallel to the b axis was used. The crystal needle axis was fixed parallel to the ω axis of the diffractometer to reduce the effect of strong absorption of EuAs_3 crystals ($\mu = 35$ cm⁻¹) synthesized with natural Eu. To obtain additional measurement of reflections hkl with $k > 2$, a second crystal of size $1 \times 1 \times 4$ mm³ with the needle axis parallel to the a axis was used. The single crystals of $(\text{EuAs}_{0.02}\text{P}_{0.98})_3$ and $(\text{EuAs}_{0.60}\text{P}_{0.40})_3$ were of similar size and were oriented similarly to that of EuAs_3 . Because of the nonavailability of large $\beta\text{-EuP}_3$ single crystals, a single-crystal plate with the flat surface parallel to the (201) plane, and of rather irregular shape, had to be used.

III. MAGNETIC ORDERING IN EuAs_3

A. Commensurate antiferromagnetic phase

EuAs_3 crystallizes with the monoclinic space group $C2/m$ and is isostructural with BaAs_3 with four formula units per C -face-centered unit cell (Table I). A neutron-diffraction experiment at 5 K revealed magnetic reflections at reciprocal points corresponding to the doubling of the c axis of the nuclear cell. All magnetic reflections are found to follow the rule $h + k = 2n + 1$ and $l = n + \frac{1}{2}$, whereas the nuclear reflections have $h + k = 2n$ and $l = n$, where n is an integer. No

TABLE II. Electrical and magnetic properties of EuAs_3 , $\text{Eu}(\text{As}_{1-x}\text{P}_x)_3$, and $\beta\text{-EuP}_3$. [Ref. 3 and Bauhofer *et al.* (unpublished)].

| Compound | Carrier density (cm ⁻³) | Θ_p (K) | | C (emu K/mol) | | μ_{eff} (μ_B) | | T_N (K) | T_L (K) |
|--|-------------------------------------|----------------|-------|---------------|-------|--------------------------------|-------|-----------|-----------|
| | | [100] | [010] | [100] | [010] | [100] | [010] | | |
| EuAs_3 | 9.8×10^{20} at 3 K | -1 | 2.5 | 7.73 | 7.65 | 7.86 | 7.82 | 11.3 | 10.4 |
| $\text{Eu}(\text{As}_{0.06}\text{P}_{0.40})_2$ | 2.2×10^{19} at 3 K | 1 | a | 7.74 | a | 7.87 | a | 9.5 | 8.7 |
| $\text{Eu}(\text{As}_{0.02}\text{P}_{0.98})_3$ | 2.3×10^{18} at 3 K | 5.5 | a | 7.94 | a | 7.97 | a | 8.4 | 7.5 |
| $\beta\text{-EuP}_3$ | 2.2×10^{13} at 6.5 K | 7 | 8 | 7.69 | 7.80 | 7.84 | 7.90 | 10.0 | |

^aDeviation from linear $(1/\chi)(T)$ relation.

reflections with other combinations of indices were found. These indices correspond to a wave vector $\mathbf{k} = (-1, 0, \frac{1}{2})$. We have chosen -1 rather than 1 for obtaining a comparable wave vector to those of the other phases of EuAs_3 and $\alpha\text{-EuP}_3$. Intensities of 137 nuclear and 139 magnetic reflections were measured from the layers $h0l$, $h1l$, and $h2l$ at 5 K from a crystal needle with the elongated dimension parallel to $[010]$ fixed parallel to the ω axis of the diffractometer. 22 nuclear and 18 magnetic reflections were measured from the layers $0kl$, $1kl$, and $2kl$ from another crystal with the needle axis parallel to $[100]$. The relative intensities of the magnetic reflections showed that the Eu atoms related by the center of symmetry have parallel spins. This, together with the wave vector $(-1, 0, \frac{1}{2})$, leads to the collinear magnetic structure of Fig. 1. The absolute scale of the magnetic reflections was obtained by refining the crystal structure with nuclear reflections. This refinement led to an agreement value $R = 0.051$. The used scattering length⁹ of As was 6.73×10^{-12} cm and that for Eu was refined yielding the value 6.80×10^{-12} cm. The magnetic form factor of Eu^{2+} used was obtained by Freeman and Desclaux¹⁰ from the relativistic Dirac-Fock wave functions. The direction and the magnitude of magnetic moment of Eu atoms were determined from the structure model of Fig. 1 using the magnetic reflections. The agreement factor obtained was $R = 0.069$. The results are summarized in Table III. The magnetic moments of the Eu atoms are found to be oriented parallel and antiparallel to the monoclinic b axis of the crystal and are $6.05\mu_B$ at 5 K. The magnetic structure of the commensurate phase, stable below 10.2 K, consists of ferromagnetic $(\bar{2}01)$ planes stacked antiferromagnetically $(+ -)$.

B. Incommensurate antiferromagnetic phase

The commensurate phase which has moments parallel to b gave a strong magnetic Bragg reflection at the reciprocal point $(-1, 0, \frac{1}{2})$ indexed with respect to the chemical cell. The intensity of this reflection decreases with increasing temperature according to the square of the Brillouin function $B_{S=7/2}^2$, until at $T_L = 10.26$ K it drops abruptly to zero, suggesting a first-order transition

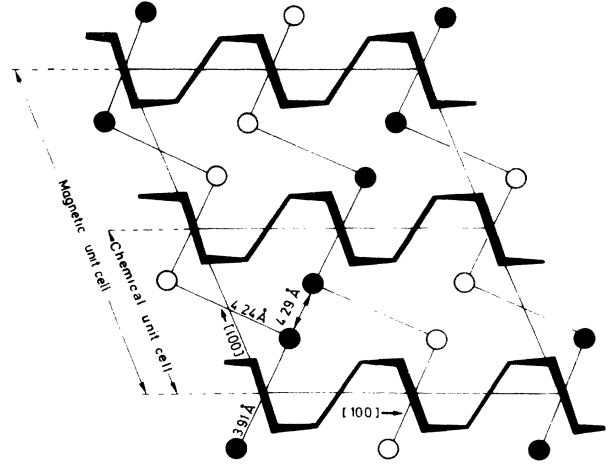


FIG. 1. Magnetic structure of the commensurate antiferromagnetic phase of EuAs_3 stable below 10.3 K. The solid and open circles represent europium atoms with opposite spin directions which are parallel to the $[010]$ direction. The puckered arsenic layers are represented schematically.

(Fig. 2). In the inset of Fig. 3, the intensities obtained in q scans parallel to c^* through the reciprocal point $(-1, 0, \frac{1}{2})$ as a function of temperature are shown. At 10.13 K only the peak belonging to the commensurate phase is observed. At 10.17 K a pair of satellites at $(-1, 0, \frac{1}{2} \pm \delta)$ starts to develop, which increases very rapidly in intensity and moves away from the commensurate peak at $(-1, 0, \frac{1}{2})$ as the temperature rises above T_L . The satellite intensity decreases again at higher temperature and can no longer be observed above 10.9 K, but the separation of the satellites increases continuously with temperature until they disappear. The component of the wave vector parallel to c^* is found to vary smoothly from an extrapolated value of 0.35 at T_N to the commensurate value $\frac{1}{2}$ at T_L . The value of the wave vector was determined in heating and cooling cycles and no significant hysteresis was observed. The temperature stability in these measurements was about ± 0.02 K and the wave vector was determined with an accuracy of

TABLE III. Magnetic structures of the different phases of EuAs_3 , $\text{Eu}(\text{As}_{1-x}\text{P}_x)_3$, and $\beta\text{-EuP}_3$. α denotes the angle between the major axis of the ellipse and the a^* direction, S_x, S_y denote components of the magnetic moments along the major and the minor axes of the ellipse, N denotes the number of independent reflections, and R is the agreement factor.

| Compound | T (K) | Wave vector | Moment direction | α (deg) | Magnetic model | | | N | R |
|--|------------|------------------------|---------------------|-------------------|----------------------|----------------------|------------------------------|-----|------|
| | | | | | S_x (μ_B) | S_y (μ_B) | S_z (μ_B) | | |
| EuAs_3 | 5.0 | $(-1, 0, \frac{1}{2})$ | $\pm[010]$ | | 0 | 0 | 6.1 | | 0.07 |
| EuAs_3 | 10.35 | $(-0.95, 0, 0.38)$ | $\pm[010]$ | | 0 | 0 | 3.3 | 95 | 0.11 |
| $\text{Eu}(\text{As}_{0.06}\text{P}_{0.40})_3$ | 5.0 | $(-1, 0, \frac{1}{2})$ | $\pm[010]$ | | 0 | 0 | 6.38(5) | 58 | 0.06 |
| $\text{Eu}(\text{As}_{0.60}\text{P}_{0.40})_3$ | 9.15 | $(-0.90, 0, 0.35)$ | $\pm[010]$ | | 0 | 0 | 2.30(1) | 64 | 0.12 |
| $\text{Eu}(\text{As}_{0.02}\text{P}_{0.98})_3$ | 4.0 | $(-0.726, 0, 0.222)$ | in (010) plane | 99(1) | 7.3(2) | 4.5(1) | 0 | 209 | 0.15 |
| $\text{Eu}(\text{As}_{0.02}\text{P}_{0.98})_3$ | 7.5 | $(-0.726, 0, 0.255)$ | $\pm[010]$ | | 0 | 0 | 3.9(1) | 46 | 0.11 |
| $\beta\text{-EuP}_3$ | 2.0 | $(0, 0, \frac{1}{2})$ | $\pm[010]$ | | 0 | 0 | Eu(1) 7.7(1) Eu(2) 8.4(1) | 394 | 0.24 |

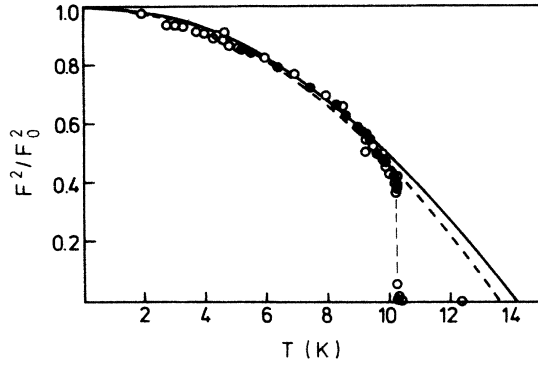


FIG. 2. Temperature dependence of the reduced intensity of the $(10\frac{1}{2})$ magnetic reflection. The squares of the Brillouin function $B_{7/2}^2$ corresponding to $T_N = 13.5$ K and 14 K are also shown. The intensity of the $(10\frac{1}{2})$ reflection decreases according to the square of the Brillouin function at lower temperature. However, the intensity drops abruptly to zero at about 10.3 K, indicating that the commensurate to incommensurate phase transition is first order.

about ± 0.01 reciprocal-lattice units.

These results show that the intermediate magnetic phase of EuAs_3 is an incommensurate antiferromagnetic phase with the wave vector approximately $(-1, 0, q_m)$ which undergoes a lock-in transition to the commensurate phase with the zone-boundary wave vector $q_m = q_0 = \frac{1}{2}$. More detailed measurements showed that the actual wave vector is $(-0.95, 0, q_m)$ in which the component parallel to a^* is almost temperature independent. No second- or higher-order satellites were observed. A second-order satellite, if it exists, has less than

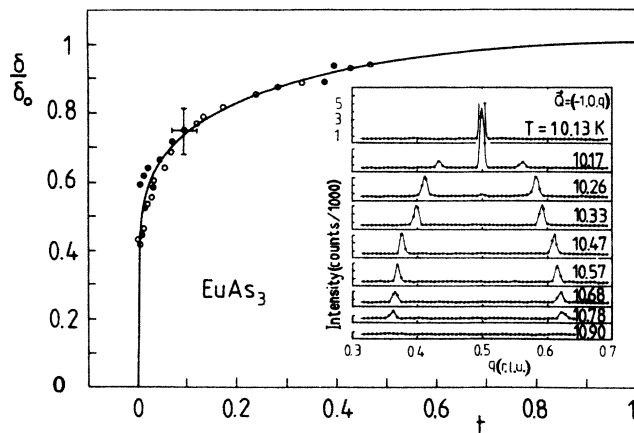


FIG. 3. Temperature dependence of the modulation part δ of the wave vector $(-1, 0, \frac{1}{2} \pm \delta)$. Open and solid circles correspond to the heating and cooling cycles, respectively. The solid line represents the results of a sine-Gordon soliton-lattice theory. Extrapolated scale value is $\delta_0 = 0.15$. The abscissa shows the reduced temperature $t = (T - T_L) / (T_N - T_L)$ where T_L and T_N refer to the lock-in and Néel temperatures, respectively. In the inset the temperature variation of the intensity of q scans parallel to c^* through $(-1, 0, \frac{1}{2})$ is shown.

5% of the intensity of the first-order satellite at 10.4 K. The intensities of 95 independent satellites were measured at 10.35 K and were found to follow quite closely the intensities of the parent reflections in the commensurate phase. A model was therefore chosen in which the relative orientations of the spin on Eu atoms within one primitive chemical unit cell is the same as in the commensurate phase, but the spins are sinusoidally modulated from cell to cell. Two forms of modulations were tried: for the first, the spin directions held in the (010) plane were sinusoidally modulated (spiral model), and in the second the amplitudes, held parallel to the [010] direction, were modulated sinusoidally (linear modulation). The second model with the spins parallel to the [010] direction gave significantly better agreement than the spiral model, and also than any other model that was tried. Using the linear model we have refined the moments of the Eu atoms obtaining an agreement factor $R = 0.11$ between observed and calculated structure factors and an amplitude of $3.3\mu_B$ for the modulated moment at $T = 10.35$ K. This corresponds to the rms moment per Eu atom of $2.3\mu_B$. The extrapolated value of moment according to the Brillouin curve at 10.35 K is $2.7\mu_B$. In the incommensurate phase we have therefore about 15% less ordered moment than would be expected if the magnetic structure remained commensurate.

Figure 3 shows the temperature dependence of the modulation vector $\delta = q_m - \frac{1}{2}$ in the heating and cooling cycles. No significant hysteresis has been observed. The solid line in Fig. 3 is the temperature variation of the modulation vector obtained from the sine-Gordon soliton-lattice model. The experimental results agree very closely with this model (see Sec. VIII).

IV. MAGNETIC ORDERING IN $\text{Eu}(\text{As}_{0.60}\text{P}_{0.40})_3$

$\text{Eu}(\text{As}_{0.60}\text{P}_{0.40})_3$ is isostructural with EuAs_3 . Specific-heat measurements¹¹ show two peaks at 9.5 and 8.5 K which look very similar to those of EuAs_3 and suggest magnetic transitions at these temperatures.

A. Commensurate antiferromagnetic phase

The low-temperature phase of $\text{Eu}(\text{As}_{0.60}\text{P}_{0.40})_3$, stable below 8.5 K, is found to be identical with that of the commensurate antiferromagnetic phase of EuAs_3 . The wave vector was found to be $(-1, 0, \frac{1}{2})$. We measured the intensities of 58 magnetic reflections at 5 K whose intensities correspond well with those of the commensurate antiferromagnetic phase. The refinement of the magnetic moment of Eu atoms using the magnetic structure model of the commensurate antiferromagnetic phase of EuAs_3 lead to a moment value of $6.38(5)\mu_B$ per Eu atom at 5 K. The agreement factor for this factor was $R = 0.064$. The scale factor was obtained from the refinement of the nuclear structure with 101 independent reflections leading to an agreement factor $R = 0.055$. We have determined the temperature variation of the intensity of the $(-10\frac{1}{2})$ reflection which behaves similarly to that found in EuAs_3 . At low temperature it follows

the Brillouin function for $J = \frac{7}{2}$. However, at $T = 8.9$ K there is a discontinuity corresponding to the first-order transition to the intermediate incommensurate phase.

B. Intermediate incommensurate phase

We expected that the intermediate incommensurate phase in $\text{Eu}(\text{As}_{0.60}\text{P}_{0.40})_3$ would be similar to that of EuAs_3 . Neutron-diffraction measurements showed the intermediate magnetic phase in $\text{Eu}(\text{As}_{0.60}\text{P}_{0.40})_3$ to be an incommensurate phase with the wave vector $(-0.90, 0, 0.35)$ at 9.5 K. As in the case of EuAs_3 , the component of the wave vector parallel to a^* is found to be almost temperature independent—its deviation from unity [0.10 reciprocal lattice unit (r.l.u.)] being larger than that (0.05 r.l.u.) of EuAs_3 . Figure 4 shows the temperature variation of the intensities of the satellites obtained in q scans approximately parallel to c^* through $(-1, 0, \frac{1}{2})$. The component of the wave vector parallel to c^* is found to be temperature dependent, but not as strongly as in the case of EuAs_3 (Fig. 5). The temperature dependence is almost linear with a pronounced first-order lock in to the commensurate antiferromagnetic phase at about 8.9 K. The substitution of 40% of As by P in EuAs_3 has completely destroyed the soliton-lattice behavior found in EuAs_3 and converted it to a linear behavior. No second- or higher-order harmonics have been observed. We have measured the intensities of 64 satellites at 9.15 K. The incommensurate structure is found to be similar to that of the incommensurate magnetic structure of EuAs_3 , apart from the slightly different modulation direction. The refinement of the magnetic moment (sine-wave modulation $\mathbf{m} \parallel \mathbf{b}$) leads to an agreement factor $R = 0.119$ between the observed and calculated intensities. The amplitude of the magnetic moment was found to be $2.30(1)\mu_B$ per Eu atom at 9.2 K. This corresponds to the rms moment per Eu atom of $1.62\mu_B$.

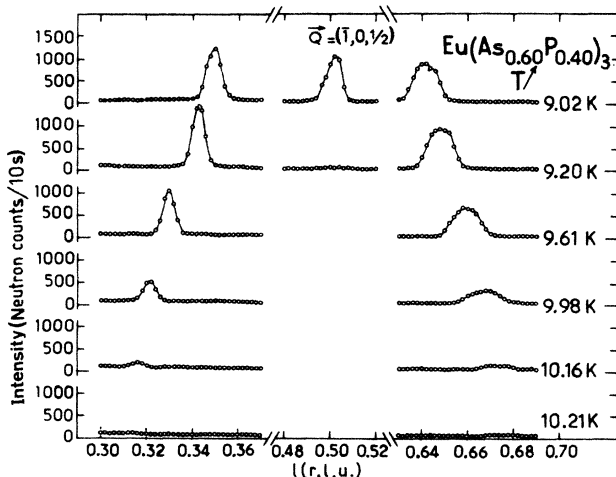


FIG. 4. Temperature variation of the intensity obtained in q scans approximately parallel to c^* through $(-1, 0, \frac{1}{2})$.

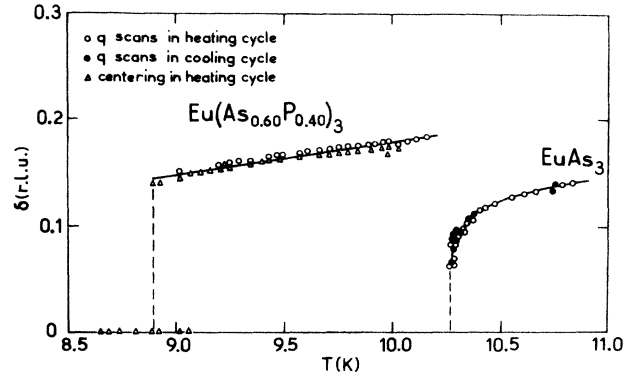


FIG. 5. Comparison of the temperature dependence of the modulation vector δ of EuAs_3 and $\text{Eu}(\text{As}_{0.60}\text{P}_{0.40})_3$. Crossover from the sine-Gordon soliton-lattice behavior for EuAs_3 to a linear behavior for $\text{Eu}(\text{As}_{0.60}\text{P}_{0.40})_3$ is demonstrated.

V. MAGNETIC ORDERING IN $\text{Eu}(\text{As}_{0.02}\text{P}_{0.98})_3$

EuP_3 has two modifications. α - EuP_3 is isostructural to EuAs_3 and is stable above 960 K. The α phase can be quenched to a metastable phase at room temperature or can be stabilized at room temperature by adding a small amount (2%) of As. β - EuP_3 is thermodynamically stable below 960 K and has a modified crystal structure. Since it is difficult to grow pure α - EuP_3 single crystals we have chosen to study $\text{Eu}(\text{As}_{0.02}\text{P}_{0.98})_3$ which can be grown more easily. The magnetic behavior of this solid solution is expected to be similar to that of pure α - EuP_3 . Like EuAs_3 , $\text{Eu}(\text{As}_{0.02}\text{P}_{0.98})_3$ shows two anomalies in the specific heat,¹¹ magnetic susceptibility,^{2,3} and resistivity,^{2,3} one at 8.5 K and the other at 7.4 K, which are presumably associated with magnetic ordering.

A. Low-temperature incommensurate phase

A neutron-diffraction experiment was performed at 4.2 K to determine the magnetic structure of the low-temperature ordered phase stable below 7.4 K. By analogy with EuAs_3 , a commensurate antiferromagnetic phase was expected. However, no magnetic intensity was found at positions corresponding to a simple commensurate antiferromagnetic structure. Further search revealed magnetic satellites in incommensurate positions near to those corresponding to the commensurate antiferromagnetic phase of EuAs_3 . The wave vector was determined from the mean positions of several strong magnetic reflections and was found to be $\mathbf{k} = (-0.726, 0, 0.222)$. Intensities of 209 independent reflections determined from two crystal needles with needle axes parallel to b and a axes of the crystal were measured at 4 K. Two structure models were tried: (a) the spin orientations, held in the (010) plane, are sinusoidally modulated (spiral elliptic model), and (b) the amplitude of the spins held parallel to the [010] direction are modulated sinusoidally (see Appendix A). In these models the relative orientations of the spins on Eu atoms in one chemical cell are the same as in the commensurate

antiferromagnetic phase of EuAs_3 but are modulated from cell to cell. Model (a) gave a significantly better agreement factor $R=0.15$ compared to the $R=0.21$ for model (b). The components of the magnetic moments refined with model (a) are $S_x=7.3(2)\mu_B$, $S_y=4.5(1)\mu_B$, and the angle α between the a^* axis and S_x is refined to be $\alpha=99(1)^\circ$ (Table III). The major axis of the ellipse therefore makes an angle of 9° from the crystallographic c axis.

Figure 6 shows the temperature variation of the intensity of the $(-0.73, 0, 0.25)$ reflection. The intensity of this reflection decreases continuously as the temperature is raised. However, at 7.5 K a discontinuity in intensity is observed. This corresponds well to the anomaly observed in the specific heat at about the same temperature. The magnetic phase transition at $T=7.5$ K is therefore first order. Between 7.5 K and $T_N=8.5$ K, the intensity variation is found to be continuous and corresponds to a second-order phase transition at T_N . In the same figure temperature variation of the component of the wave vector parallel to c^* is shown. This component of the wave vector increases continuously from a low-temperature value of about 0.22. At $T=7.5$ K it undergoes an abrupt increase from 0.24 to 0.26 corre-

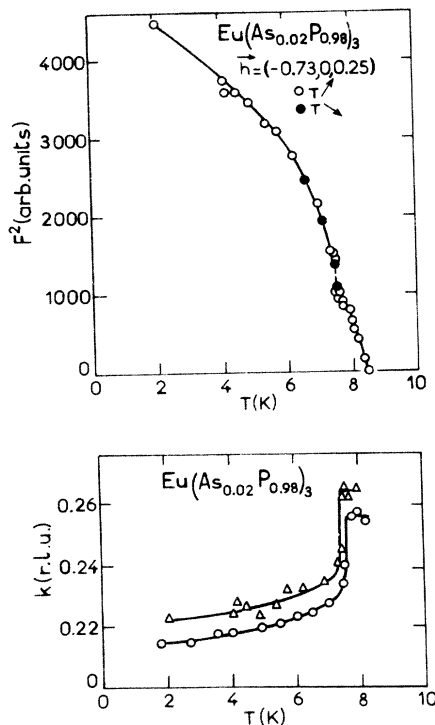


FIG. 6. Temperature variation of the intensity of $(-0.73, 0, 0.25)$ magnetic reflection of $\text{Eu}(\text{As}_{0.02}\text{P}_{0.98})_3$. A discontinuity in intensity is observed at $T=7.5$ K corresponding to a first-order phase transition from sine-wave to helical modulation. At $T_N=8.5$ K a second-order phase transition is observed. Temperature variation of the component k of the wave vector $(-0.75, 0, k)$ is shown below. k increases with increasing temperature and at $T=7.5$ K, k increases discontinuously from 0.24 to 0.26. The circles and triangles represent two independent sets of measurements.

sponding to the first-order magnetic phase transition from the lower-temperature incommensurate phase to the intermediate incommensurate phase. The component of the wave vector parallel to a^* is found to be temperature independent.

B. Intermediate incommensurate phase

The wave vector of the intermediate incommensurate phase was found to be $\mathbf{k}=(0.726, 0, 0.255)$. Intensities of 46 independent reflections were measured from two crystals at 7.5 K. The sine-wave amplitude modulation (spin direction parallel to $[010]$ or $[0\bar{1}0]$) described in Sec. V A gave the best agreement factor $R=0.11$ compared to the $R=0.28$ obtained using the spiral elliptic model. The amplitude of the modulated moment obtained using the sine-wave amplitude modulation is $3.9(1)\mu_B$ (rms value $2.8\mu_B$) (Table III).

The first magnetic phase in $\text{Eu}(\text{As}_{0.02}\text{P}_{0.98})_3$ below $T_N=8.5$ K is therefore a sine-wave amplitude modulated incommensurate phase with magnetic moments parallel to the $[010]$ or $[0\bar{1}0]$ direction. At about 7.5 K the spin directions flip to the (010) plane and another incommensurate spiral phase is developed with a first-order transition. The sine wave to helimagnetic transition has been predicted theoretically for the case of weak anisotropy but has been observed for the first time to our knowledge in $\text{Eu}(\text{As}_{0.02}\text{P}_{0.98})_3$ (see Sec. IX).

VI. MAGNETIC ORDERING IN $\beta\text{-EuP}_3$

$\beta\text{-EuP}_3$ is isotypic to SrP_3 and crystallizes with the monoclinic space group $C2/m$ with the lattice constants $a=11.307(3)$ Å, $b=7.345$ Å, $c=8.453(2)$ Å, $\beta=103.39(3)$ deg and has $Z=8$ formula units per unit cell.⁸ There are two crystallographically independent Eu atoms at positions $x_1=0.2918(1)$, $y_1=0$, $z_1=0.2261(1)$ and $x_2=0.9579(1)$, $y_2=0$, $z_2=0.2590(1)$. Specific-heat, susceptibility, and resistivity measurements show that $\beta\text{-EuP}_3$ undergoes a second-order phase transition at $T_N=10$ K ordering in a single step.^{2,3} To determine the nature of magnetic ordering at $T < T_N$ neutron-diffraction measurements were performed at 2 K. A single-crystal plate of rather irregular shape with its flat surface parallel to the $(\bar{2}01)$ plane was used with its b axis set parallel to the ω axis of the diffractometer. Magnetic reflections were observed at positions corresponding to the doubling of the c axis of the nuclear cell. The magnetic reflections observed obey the rule $h+k=2n$, $l=n+\frac{1}{2}$ and therefore correspond to a wave vector $\mathbf{k}=(0, 0, \frac{1}{2})$. Intensities of 351 nuclear and 354 magnetic reflections were measured at 2 K. The determination of the magnetic structure reduces to the problem of determining the relative phases of four Eu atoms (the two symmetry-inequivalent Eu atoms and the other two Eu atoms related to the former by centers of inversion) and their moment orientations. The above problem is solved directly by using the spin Patterson function¹² as has been illustrated in Fig. 7 (see also Appendix B). In the plot of the nuclear Patterson function, peaks are clearly seen at A given by the vector $d(\text{Eu}(1)\text{-Eu}(2))$ and

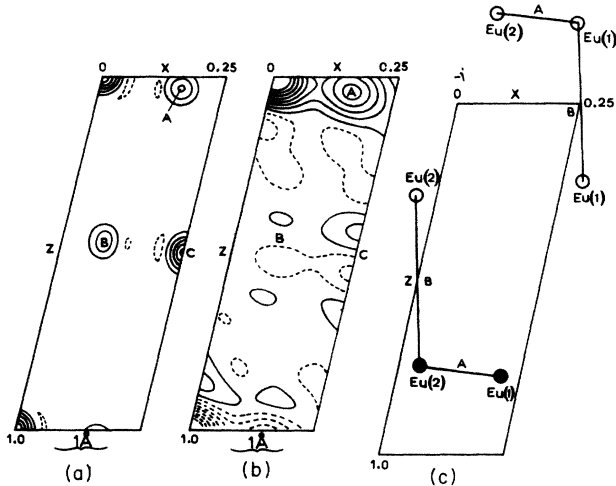


FIG. 7. Comparison of the (a) nuclear and (b) magnetic Patterson functions for β -EuAs₃ projected down [010]. Contours are drawn at equal arbitrary intervals. The europium positions in the underlying chemical structure and the vectors giving rise to the Patterson peaks at A and B are indicated in (c) as are the relative orientations of the spins in the magnetic structure deduced. The solid and open circles show oppositely directed spins.

at B from the superposition of peaks from Eu(1) atoms related by the center of inversion at $(\frac{1}{4}\frac{1}{4}0)$, and Eu(2) atoms related by the center of inversion at $(00\frac{1}{2})$. The third independent peak at C is the superposition of four $d(\text{Eu}(1)\text{-Eu}(2))$ vectors. In the magnetic Patterson function the peak at A is clearly positive and approximately circular, and at B it is hardly evident, indicating the superposition of positive and negative contributions. The observation that it is positive on the side corresponding to $d(\text{Eu}(1)\text{-Eu}(2))$ and negative on the other side suggests that the center at $(\frac{1}{4}\frac{1}{4}0)$ does not reverse the moment direction whereas that at $(00\frac{1}{2})$ does. The large peak at A clearly corresponds to parallel coupling of Eu(1) and Eu(2). These considerations lead to the magnetic structure of Fig. 6(c) with the moment direction parallel to [010] and the magnetic space group is $C2/m$ with no time-reversal operators. The magnetic reflections were placed on an absolute scale by refining the nuclear structure with the structure factors corrected for the strong absorption of the irregular plate crystal. The scattering length used for P atoms was 5.13×10^{-13} cm. The magnetic moments on the two Eu atoms and the three direction cosines of the moment directions with respect to the crystallographic axes were refined with the intensities of the magnetic reflections placed in the absolute scale. The refined parameters are given in Table III. The magnetic moments of the Eu atoms are found to be oriented along the monoclinic b axis of the crystal and the average moment per Eu atom obtained by refinement is $7.91\mu_B$. The agreement factor obtained is $R=0.24$. Although the agreement factor is rather high, it is comparable to the nuclear agreement factor and is the best

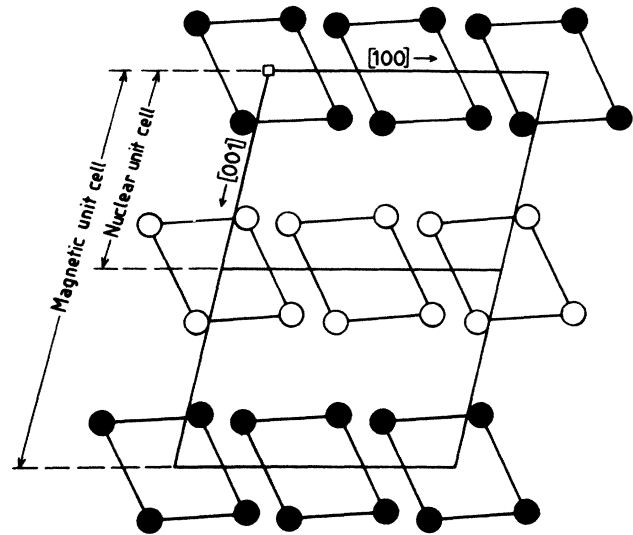


FIG. 8. Schematic representation of the magnetic structure of β -EuP₃. The solid and open circles represent Eu atoms with opposite moment directions which are parallel to the b axis. The As atoms are not shown.

agreement factor of all models which were tried. We attribute the poor agreement to inaccuracy in the absorption corrections due to the difficulty of obtaining a good description of the irregularly shaped plate crystal. Figure 8 shows the magnetic structure of β -EuP₃. The structure consists of approximate ferromagnetic planes parallel to the (001) planes coupled in the sequence (+ + - -).

Figure 9 gives the temperature dependence of the intensity of the $(00\frac{1}{2})$ magnetic reflection. The intensity of this reflection decreases continuously with temperature and becomes negligibly small at $T_N=10$ K. The

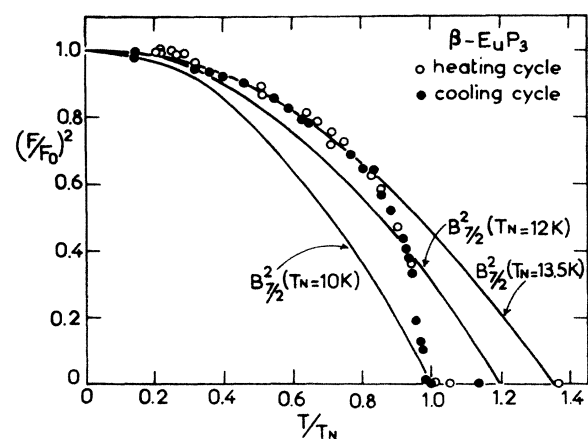


FIG. 9. Temperature variation of the reduced intensity of the $(00\frac{1}{2})$ magnetic reflection of β -EuP₃ in the heating (open circles) and in the cooling cycle (solid circles). The solid curves represent the squares of the Brillouin functions $B^2_{7/2}$ corresponding to T_N 10, 12, and 13.5 K.

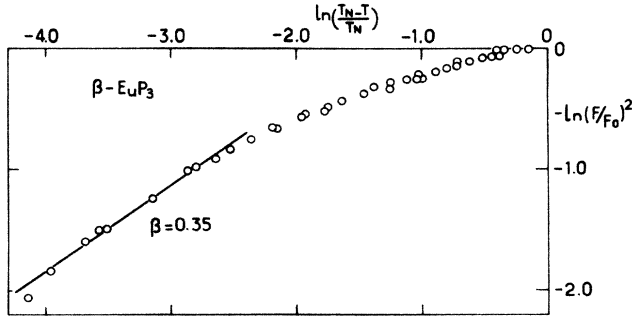


FIG. 10. $\ln(F/F_0)^2$ vs $\ln[(T_N - T)/T_N]$ plot of the $(00\frac{1}{2})$ magnetic reflection of β -EuP₃. The critical exponent β is found to be 0.35 which is close to the value $\beta=0.313$ expected for the three-dimensional Ising model or $\beta=0.365$ for the three-dimensional Heisenberg model.

paramagnetic-to-antiferromagnetic phase transition is therefore second order in agreement with the result of specific-heat measurement. However, the intensity variation does not follow the square of the Brillouin function corresponding to $S = \frac{7}{2}$. In Fig. 6 plots of the square of the Brillouin function $B_{7/2}^2$ for the actual $T_N = 10$ K and two other hypothetical temperatures $T_N = 12$ and 13.5 K are shown. The intensity of the $(00\frac{1}{2})$ magnetic reflection agrees rather well with $B_{7/2}^2$ ($T_N = 13.5$ K) for $T < 8$ K. In the temperature range 8–10 K, the intensity drops more rapidly than in $B_{7/2}^2$ ($T_N = 13.5$ K). However, the variation is continuous. A very rough estimation of the critical exponent has been attempted and is shown in Fig. 10. The critical exponent obtained is $\beta = 0.35$, which is about the same as that expected for the three-dimensional Ising model ($\beta \approx \frac{5}{16} = 0.313$), or for the three-dimensional Heisenberg model ($\beta \approx 0.365$).

VII. EXCHANGE MODEL AND THE PHASE DIAGRAM OF THE FIRST MAGNETIC PHASE OF EuAs₃ BELOW T_N

We have performed model calculations to gain some insight into the origin of the modulated structure. They are based on an anisotropic Heisenberg exchange

$$H_{\text{ex}} = -\frac{1}{2} \sum_{\substack{l, l' \\ \alpha, \alpha'}} J_{ll'}^{\alpha\alpha'} \mathbf{S}_l^\alpha \cdot \mathbf{S}_{l'}^{\alpha'} \quad (1)$$

(l, l' = unit cell; $\alpha, \alpha' = 1-4$: basis atom). The neighbors of any Eu²⁺ ion can be separated into a nearest-neighbor (NN) group (distance $\sim 3.01-4.29$ Å) and a next-NN (NNN) group (distance 5.76–5.99 Å). From inspection of the commensurate antiferromagnetic phase in Fig. 11 we conclude that the exchange-interaction constants I_0 , $I_1 > 0$ for the NN exchange and $I_2 < 0$ for the NNN exchange. The former is assumed to be anisotropic for coupling in and out of the ferromagnetic $(\bar{2}01)$ plane. Note that neighboring $(\bar{2}01)$ planes are coupled both ferro- (I_0) and antiferromagnetically (I_2), whereas coupling to the second-nearest neighbor planes is neglected

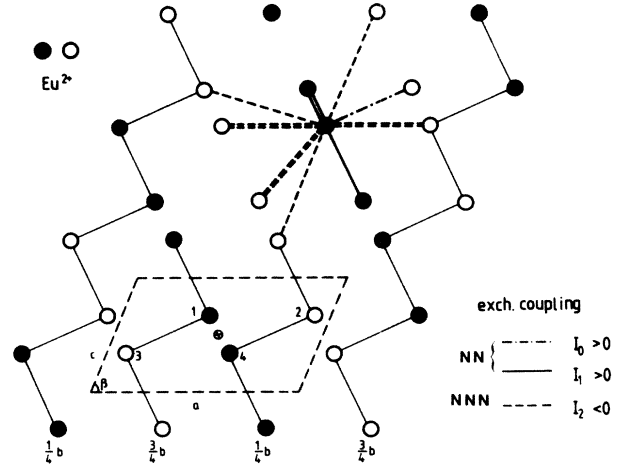


FIG. 11. Crystal structure and magnetic low-temperature phase of EuAs₃. (As atoms are not shown.) Chemical unit cell (atoms 1–4, basis vectors $\mathbf{a}, \mathbf{b}, \mathbf{c}$) is indicated by dotted lines; \mathbf{b} is perpendicular to the plane. The reciprocal lattice is denoted by $\mathbf{a}^*, \mathbf{b}^*, \mathbf{c}^*$. Crossed circle corresponds to the inversion center. Magnetic moments are parallel (open circles) and antiparallel (solid circles) to \mathbf{b} . Exchange coupling: double lines indicate coupling to Eu atoms $\pm \frac{1}{2}\mathbf{b}$ above and below center atom ($a = 9.43$ Å, $b = 7.50$ Å, $c = 5.75$ Å, $\beta = 67.5^\circ$).

since Eu distances become rather large (≥ 8 Å) for them. Because the moments are pointing along the $\pm \mathbf{b}$ directions for all temperatures below T_N , a sufficiently strong anisotropy potential $\sim D[S_y^2 - \frac{1}{3}S(S+1)]$ must also exist which is, however, not included explicitly. To predict the first magnetic phase as stable immediately below T_N we calculate the paramagnetic susceptibility

$$\chi_\kappa^{-1}(\mathbf{q}) = [T - C\bar{I}_\kappa(\mathbf{q})]/C, \quad C = \frac{1}{3}S(S+1) \quad (2)$$

where $\kappa = 1-4$ refers to one of the normal spin coordinates $S_\kappa(\mathbf{q})$ which diagonalize the exchange tensor

$$I_{\alpha\alpha'}(\mathbf{q}) = N^{-1} \sum_{l, l'} J_{ll'}^{\alpha\alpha'} \exp[i\mathbf{q} \cdot (\mathbf{R}_l - \mathbf{R}_{l'})].$$

The $\bar{I}_\kappa(\mathbf{q})$ are the resulting diagonal components referred to as “exchange bands.” The first stable magnetic phase is determined by the singularity in $\chi_\kappa(\mathbf{q})$, i.e., by the maximum $I_\kappa(\mathbf{q}_m)$ in the topmost exchange band which also determines $T_N = CI_\kappa(\mathbf{q}_m)$. The spin modulation is described by the normal coordinate $S_\kappa(\mathbf{q}_m)$. For $\mathbf{q} = \mathbf{q}\mathbf{c}^*$ along the observed modulation direction, the $S_\kappa(\mathbf{q})$ result from a pairwise hybridization of collective coordinates $S_\lambda^0(\mathbf{q})$ ($\lambda = 1-4$), $S_1(\mathbf{q}) = a_1(\mathbf{q})S_1^0(\mathbf{q}) + b_1(\mathbf{q})S_2^0(\mathbf{q})$, etc. The ordering in $\kappa = 1-4$ corresponds to decreasing $\bar{I}_\kappa(\mathbf{q})$. The components (S_1^0, S_2^0) of the critical coordinate $S_1(\mathbf{q})$ are shown in the inset of Fig. 12. Computation of $\bar{I}_\kappa(\mathbf{q})$ as a function of the exchange parameters (I_0, I_1, I_2) and search for the \mathbf{q} position of the absolute maximum $I_\kappa(\mathbf{q}_m)$ and symmetry of its eigenvector lead to a global phase diagram of the first stable magnetic phase in the (r, r') plane. Here

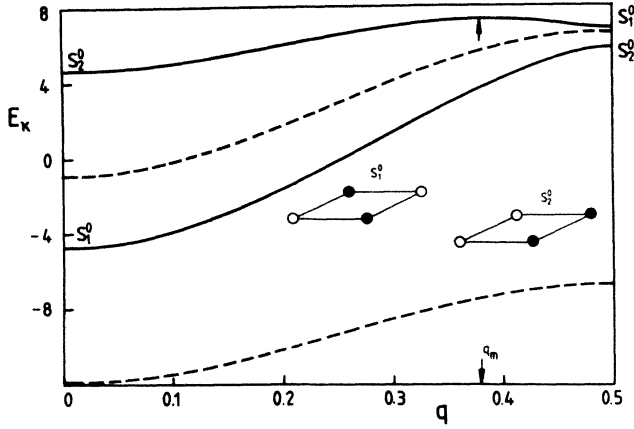


FIG. 12. Exchange bands $E_k = \bar{I}_k(q)/I_1$ for $q = qc^*$ and exchange parameters $[(r, r') = (1.6, 5.7)]$. Absolute maximum (arrow) corresponds to modulation vector $q_m = 0.38$ ($\delta = 0.12$). Symmetry of some bands is indicated. Broken bands have S_3^0, S_4^0 symmetry.

$r = (-I_2/I_1) > 0$ is the “competition ratio” and $r' = (I_0/I_1) > 0$ the “anisotropy ratio.” The shape of exchange bands depends on r, r' and I_1 defines the scale. In Fig. 12 they are shown for an (r, r') set which leads to an absolute maximum at an incommensurate vector q_m . Its very existence is due to hybridization of $S_1^0(q), S_2^0(q)$, as can be concluded from the symmetry exchange along q . The resulting first stable magnetic phase diagram is shown in Fig. 13. An incommensurate phase (IC) is only possible in a sector of the (r, r') plane with $r > 1, r' > 4$ necessary, but not sufficient, conditions. The incommensurate vector $\mathbf{q}_m = q_m \mathbf{c}^*$ in this sector is given by

$$q_m = \frac{1}{2\pi} \cos^{-1} \left[\frac{(1+r)(r'-r+2)}{8r^2} - \frac{1+r}{2(r'-r-2)} - \frac{r'-r-2}{2(1+r)} \right]. \quad (3)$$

Numerically $\delta = \frac{1}{2} - q_m \lesssim 0.145$ in the incommensurate sector, which is close to the extrapolated experimental value $\delta_0 = \delta(T_N) = 0.15$.

Below the incommensurate sector, the calculated first stable magnetic phase is a commensurate phase with $\mathbf{q}_0 = \frac{1}{2}\mathbf{c}^*$ and is identical with the first observed antiferromagnetic phase (AF1) for $T < T_L$. Above the incommensurate region the first stable magnetic phase is a different antiferromagnetic structure (AF2) not observed. In addition, a small ferromagnetic (FM) region exists. For isotropic NN exchange ($r' = 1$) only a FM or AF1 phase, but no modulated structure, can exist. This means that in EuAs_3 the coupling between ferromagnetic ($\bar{2}01$) planes is stronger than the coupling within the planes. This is opposite to the situation in the cerium monopnictides. The ratios r and r' cannot yet be determined unambiguously. Comparison with susceptibility data³ suggests that (r, r') lies in the lower part of the incommensurate sector. Choosing $(r, r') = (1.6, 5.7)$ as a compromise one obtains $\delta_0 = 0.12$. Fixing I_1 by $T_N = C\bar{I}_1(q_m)$ we have

$$I_0 = 1.66 \text{ K}, \quad I_1 = 0.29 \text{ K}, \quad I_2 = -0.47 \text{ K}.$$

These exchange constants are similar in magnitude to those found in the Eu monochalcogenides. The out-of-plane coupling I_0 is rather large. It should perhaps be considered as an effective coupling constant which also includes the influence of a ferromagnetic coupling to the second-nearest ($\bar{2}01$) planes (see Fig. 11), so that the real I_0 would be smaller than given above.

VIII. DISCUSSION

Due to the existence of competing interactions, $4f$ and $5f$ systems with local moments often exhibit modulated magnetic structures with a temperature-dependent modulation vector \mathbf{q}_m . Two cases are familiar: (a) “staircase behavior” where $\mathbf{q}_m(T) = (n/m)\mathbf{K}$ has only commensurate values (\mathbf{K} is the reciprocal-lattice vector; n, m are integers) as, for example, in CeSb and CeBi ; (b) genuine incommensurate structures with smooth temperature behavior and a possible lock in at a commensurate wave vector \mathbf{q}_0 at low temperatures. Examples are the heavy rare-earth (RE) metals. In the simplest case, if there is a sufficiently strong anisotropy which aligns the moments along an easy axis, a smooth temperature dependence of $\mathbf{q}_m(T)$ is obtained within the “soliton-lattice” model¹³ based on a Landau expansion of the free energy in terms of the incommensurate uniaxial order parameter

$$S(\mathbf{r}) = A e^{i\phi(z)} e^{iq_0 r}, \quad (4)$$

where $\phi(z)$ describes the moment modulation along the c axis of the crystal. This approach leads to a continuous

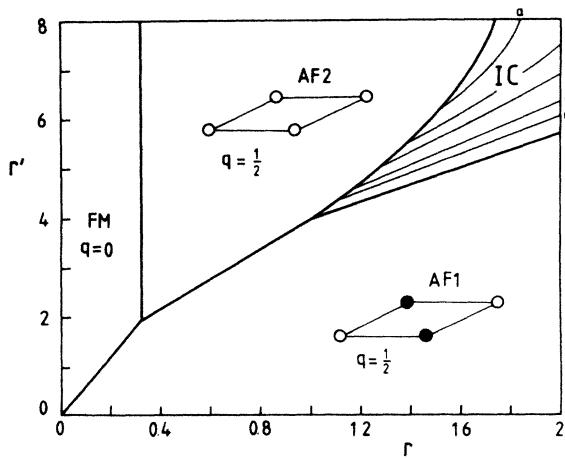


FIG. 13. Phase diagram for $T \leq T_N$ in the (r, r') parameter plane. AF1, AF2 are different antiferromagnetic commensurate phases. FM denotes the ferromagnetic phase, and IC the incommensurate phase. The IC region is shown with contours for $\delta(r, r') = \frac{1}{2} - q_m$ [cf Eq. (3)]. Curves (a)–(e): $\delta = 0.14, 0.13, 0.12, 0.11, 0.10$, respectively.

variation of $\delta(T) = \mathbf{q}_m(T) - \mathbf{q}_0$ determined by the number of phase solitons in $\phi(z)$. Because in the heavy RE metals ordering is usually not of the uniaxial type, it cannot be applied there. The condition for having a one-component order parameter ($\mathbf{S} \parallel \mathbf{y}$) immediately below T_N is $I(\mathbf{q}_m) - I(\mathbf{0}) < |D|$ where $D < 0$ is the strength of the anisotropy potential

$$D \sum_i [S_y^2(i) - \frac{1}{3}S(S+1)]$$

and $I(\mathbf{q})$ the Fourier transform of the exchange interaction. This seems to be the case in EuAs_3 because $\mathbf{m} \parallel [010]$ for all temperatures.

A. Incommensurate EuAs_3 with zone-boundary lock in

The conditions for the existence of an incommensurate phase in EuAs_3 were investigated in Sec. VII and found to imply competition between NN exchange interactions ($I_0, I_1 > 0$) and NNN interactions ($I_2 < 0$) as well as a strong anisotropy within the NN interactions: $I_1 \gg I_0$. In this case one obtains a modulated structure of the type observed with a modulation wave vector in the range $\delta = 0.1 - 0.14$ in reasonable agreement with the experimental $\delta_0 = \delta(T_N) = 0.15$. Because the commensurate lock-in temperature $T_L = 10.3$ K is close to $T_N = 11.3$ K, one has $(T_N - T_L)/T_N = 0.1$ and therefore a Landau expansion of the free energy in terms of the order parameter in Eq. (8) should be valid. One obtains the "sine-Gordon" functional

$$F[\phi] = A^2 \int dz \left\{ \frac{1}{2} [\phi'(z) - \delta_0]^2 + v [1 - \cos 4\phi(z)] \right\}, \quad (5)$$

with $v \sim A^2 \sim (T_N - T)$ which has to be minimized with respect to $\phi(z)$. The average incommensurate wave number is then given by

$$\delta(T) = \frac{1}{L} \int_{-L}^L \phi(z) dz. \quad (13)$$

As a function of $t = (T - T_L)/(T_N - T_L)$, $\delta(t)$ has a universal temperature dependence given by $\delta(t) \sim |\ln t|^{-1}$ for $t \rightarrow 0$ which is shown in Fig. 3 together with the experimental data for EuAs_3 ; the agreement is very good over the whole temperature range. It is not immediately obvious why the sine-Gordon functional describes the $\mathbf{q}_0 = \frac{1}{2}\mathbf{c}^*$ zone-boundary lock in in EuAs_3 . Because gradients of the "exchange bands" $\bar{I}_\kappa(\mathbf{q})$ ($\kappa = 1-4$; there are 4 atoms/unit cell) vanish at the zone boundary, one would expect that $F[\phi]$ contains only even powers of $\phi'(z)$. However, in the present case the symmetry of the normal coordinate

$$S_1(q) = a_1(q)S_1^0(q) + b_1(q)S_2^0(q)$$

corresponding to the topmost exchange band is itself \mathbf{q} dependent with a nonvanishing gradient of $b_1(\mathbf{q})$ at $\mathbf{q} = \frac{1}{2}\mathbf{c}^*$. Therefore, linear terms in $\phi'(z)$ are present in $F[\phi]$ so that Eq. (9) is the proper functional. The lock-in commensurate transition is caused by the (negative) "lattice energy" $\sim v$ in Eq. (5) which is due to umklapp terms with $\mathbf{K} = 2\mathbf{q}_0$ in the free-energy expansion. In EuAs_3 it is obviously energetically more favorable to

maintain a uniaxial order parameter and form a lattice of phase solitons along the modulation axis than to make a transition to a spiral-type ordering as temperature is lowered. This can again be attributed to the influence of the anisotropy potential. Taking the spin-flop (SF) fields⁷ ($\mathbf{H} \parallel \mathbf{b}$) of $H_{\text{SF}} \sim 1-2$ T as a rough measure for the anisotropy constant D , one has $|D| \simeq 0.6-1.2$ K. This has to be compared to $\bar{I}_1(q_m) - \bar{I}_1(0)$ which for the EuAs_3 exchange model⁵ chosen is about 0.7 K. Thus D is just large enough to cause uniaxial ordering. This argument is probably still true for a small temperature range below T_N , i.e., in the whole intermediate range down to T_L . Although the soliton-lattice (SL) picture explains $\delta(t)$ very well, there are some problems with this interpretation:

(i) It seems that the lock-in transition at T_L is not really continuous but is ultimately of first order. However, the $\delta(t)$ function of the SL model which is in principle continuous for $t \rightarrow 0$ ($T \rightarrow T_L$) is virtually indistinguishable from a discontinuous first-order lock-in transition because of the logarithmic behavior of $\delta(t)$. For example, when $\delta(t)/\delta_0 \simeq 0.4$ (last experimental points in Fig. 3) one has $t \simeq 10^{-3}$ for the theoretical curve, i.e., T is extremely close to the continuous lock-in temperature. Furthermore, interaction of spins with the lattice might indeed lead to a lock-in transition which is of first order.

(ii) If the temperature decreases appreciably below T_N , secondary satellites due to higher harmonics of the distorted phase $\phi(z)$ in the SL model should, in principle, occur. As mentioned above they have not been identified; possibly their intensity is too low unless one is close to T_L . In fact just before lock in a splitting of the primary incommensurate satellite into a double-peak structure was observed. This point needs further experimental investigation. Despite these reservations the soliton-lattice model seems to be the most attractive one to explain the T -dependent modulation vector in the incommensurate phase.

In conclusion, EuAs_3 is a new incommensurate antiferromagnet which belongs to a class of magnetic layered compounds that promise to be as exciting as the Ce monopnictides. Although the commensurate lock-in transition happens at the zone boundary, the modulation vector shows a nearly continuous T dependence which is adequately described by the SL model. Further investigation into the role of anisotropy of the exchange coupling and its origin, possibly by inelastic neutron scattering experiments, is necessary.

B. Incommensurate intermediate phase in $\text{Eu}(\text{As}_{1-x}\text{P}_x)_3$

The intermediate incommensurate phase has been observed in $\text{Eu}(\text{As}_{1-x}\text{P}_x)_3$ for $x \leq 0.98$. The Néel temperature T_N and the lock-in temperature T_L continuously decrease with the phosphorus concentration x . The sine-wave amplitude modulation remains for all values of x with the direction of the magnetic moments parallel and antiparallel to the [010] direction. As mentioned before, the wave vector $(q_x, 0, q_m)$ of the incommensurate phase has a q_x component which differs slightly from unity. This deviation increases with the concentration

x of P atoms. For pure EuAs_3 $\mathbf{k} = (-0.95, 0, q_m)$, for $\text{Eu}(\text{As}_{0.60}\text{P}_{0.40})_3$ $\mathbf{k} = (-0.90, 0, q_m)$, and for $\text{Eu}(\text{As}_{0.02}\text{P}_{0.98})_3$ $\mathbf{k} = (-0.726, 0, q_m)$. The deviation of the modulation direction from the c^* axis therefore increases with the concentration x of the P atoms. Another important aspect is the temperature dependence of the wave vector. As has been mentioned in Sec. VII A the temperature dependence of the modulation vector of the incommensurate phase of EuAs_3 follows the prediction of the sine-Gordon soliton-lattice theory. We have demonstrated in Fig. 5 that this behavior is destroyed for the concentration $x = 0.40$ of P atoms and is converted to a linear behavior. Obviously for $x = 0.40$ the sine-Gordon soliton-lattice theory is no longer valid. It is possible that the theory due to Bruce, Cowley, and Murray¹⁴ is more appropriate in this case. The first-order nature of the lock-in transition is more pronounced in accordance with the above-mentioned theory.¹⁴ The linear variation of the modulation vector is also observed in EuAs_3 under a hydrostatic pressure of about 4 kbar.¹⁵ The microscopic origin of this crossover from soliton-lattice to linear behavior is, however, not clear.

C. Sine-wave to helical transition in $\text{Eu}(\text{As}_{0.02}\text{P}_{0.98})_3$

For $\text{Eu}(\text{As}_{0.02}\text{P}_{0.98})_3$ we do not observe a lock-in transition from the sine-wave modulated phase to a commensurate phase such as has been observed in EuAs_3 and in $\text{Eu}(\text{As}_{1-x}\text{P}_x)_3$ for x up to $x = 0.40$ and for which the direction of the magnetic moment is parallel or antiparallel to the [010] direction. Instead, the first magnetic phase at T_N , which is a sine-wave modulated phase with the magnetic moment parallel to [010] or [010], undergoes a first-order phase transition to a helical phase in which the magnetic moments are modulated in the (010) plane. According to group theory¹⁶ for orthorhombic or lower symmetry the irreducible representations are only one dimensional and therefore, in theory, helimagnetic ordering cannot develop with a second-order phase transition. This is in accordance with the observation for EuAs_3 and $\text{Eu}(\text{As}_{1-x}\text{P}_x)_3$ for which the phase transition at T_N is second order. However, with purely isotropic exchange interactions and a single-ion anisotropy of easy-plane type the energies of two-order parameters can be accidentally degenerate and a linear combination of these two order parameters can lead to a helical structure which has the same energy as the sine-wave modulation. In this case the phase transition should be either of first order or rather complex with two successive phase transitions. Let us consider the case of an easy plane with the wave vector within the plane. In this case, even for an isotropic system, the dipolar energy makes the energy of \mathbf{m}_k^\perp , the component perpendicular to \mathbf{k} , less than that of the parallel component \mathbf{m}_k^\parallel . Then at T_N the system prefers to adopt a sine-wave modulation. As the temperature is decreased a transition to a helical structure must occur as it has a lower energy at low temperatures. This transition can be very close to T_N when isotropic exchange interactions dominate anisotropic ones. This situation is fulfilled for EuAs_3 and $\text{Eu}(\text{As}_{1-x}\text{P}_x)_3$. To our knowledge the sine

wave to helimagnetic transition in $\text{Eu}(\text{As}_{0.20}\text{P}_{0.98})_3$ is the first example of such a phenomenon to be observed in any magnetic system. It is not yet understood why this transition is favored for high P-atom concentration and not for EuAs_3 and $\text{Eu}(\text{As}_{1-x}\text{P}_x)_3$ with lower values of x .

D. Exchange mechanism in $\text{Eu}(\text{Au}_{0.02}\text{P}_{0.98})_3$ and $\beta\text{-EuP}_3$

The exchange coupling in semimetallic EuAs_3 is presumably a combination of superexchange and Ruderman-Kittel-Kasuya-Yosida (RKKY) interaction. The substitution of As by P leads to a depletion of charge carriers and should change the oscillatory behavior of the exchange constants depending on the dimensions of the Fermi-surface sheets. Up to at least 60 at. % P concentration, this only leads to reduced transition temperatures T_N and T_L but does not change the type of phases observed. At 98 at. % P concentration, however, a lock-in transition to a uniaxial commensurate phase no longer occurs but rather a transition to a spiral phase is observed. This might indicate that $\bar{I}_1(q_m) - \bar{I}_1(0)$ is now larger than $|D|$ in this diluted compound.

Finally, for complete substitution, one obtains semiconducting $\beta\text{-EuP}_3$ which also has a different crystal structure. Here one has to invoke a completely different superexchange mechanism which is obviously no longer able to sustain an incommensurate phase, perhaps due to a lack of strong enough competition in the exchange constants.

The different magnetic structures of EuAs_3 and $\beta\text{-EuP}_3$ can be understood on the basis of the structural differences between the α and β phases. In Fig. 14 we compare $\beta\text{-EuP}_3$ with $\alpha\text{-EuP}_3$ to avoid effects of lattice expansion due to the larger As atoms. The crystal axes of the α and β phases are related by

$$\begin{aligned} \mathbf{a}(\beta) &= \mathbf{a}(\alpha) - 2c(\alpha), \\ \mathbf{b}(\beta) &= -\mathbf{b}(\alpha), \\ \mathbf{c}(\beta) &= \mathbf{c}(\alpha) + \frac{1}{2}\mathbf{a}(\alpha). \end{aligned} \quad (6)$$

The puckered phosphorus layers of $\alpha\text{-EuP}_3$ consist of regularly distributed 14-membered rings in contrast to small six-membered and large 22-membered rings for $\beta\text{-EuP}_3$ (see Fig. 14, upper part). As a consequence of this difference every second pair of (ferromagnetically ordered) planes of Eu atoms in $\beta\text{-EuP}_3$ is shifted by $\frac{1}{2}\mathbf{b}$ with respect to $\alpha\text{-EuP}_3$. The projections along \mathbf{b} are nearly identical for the two phases (Fig. 14, middle) as are the ferromagnetically ordered Eu planes themselves (Fig. 14, lower part). Note, that the $(\bar{2}01)$ planes for the α axes correspond to the (001) planes for the β axes.

In the α structure, each Eu atom has four ferromagnetically coupled nearest neighbors and nine next-nearest neighbors with antiferromagnetic coupling. The ferromagnetic interaction I_0 (Sec. VII) is frustrated and leads to the occurrence of incommensurate phases. The number of different exchange interactions is larger for the β structure due to the existence of two independent

Eu positions. In addition to the exchange interactions of the α phase two more ferromagnetic and one more antiferromagnetic interactions can be identified.

The average number (4.5) of nearest neighbors is larger for the β than for the α structure, whereas the opposite is true (5.5) for the next-nearest neighbors. However, the reduction in the number of antiferromagnetic couplings is not isotropic but is concentrated between every second pair of ferromagnetically ordered Eu planes. Given that the coupling between nearest-neighbor Eu atoms is nearly identical in the two structures, this represents a natural explanation of the stacking sequence $++--$ in β -EuP₃. I_0 remains frustrated in β -EuP₃ but the number of I_0 interactions is reduced by a factor of 2.

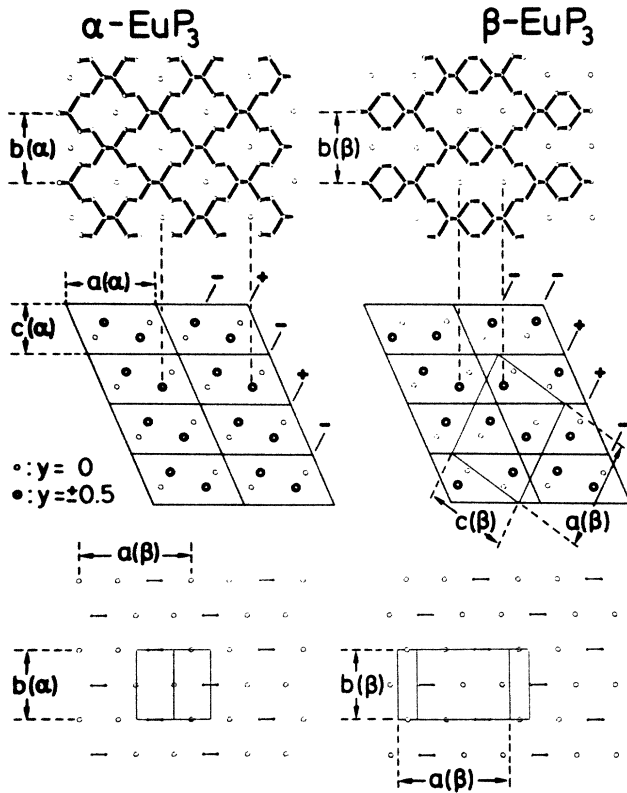


FIG. 14. Comparison of α and β structure. Top: Projections perpendicular to the phosphorus layers emphasizing the difference in catenation. This leads to a different arrangement of the Eu atoms on top of the phosphorus layers. Middle: Projections parallel to the b axes choosing the same coordinate system in both cases. The essential feature is a different distribution of Eu atoms with $y=0$ and $y=\pm 0.5$. The magnetic ordering is indicated by “+” and “-” signs. The phosphorus layers lie on the horizontal lines in this projection. Bottom: Projections on ferromagnetic Eu planes, $(\bar{2}01)$ for α axes and (001) for β axes. The Eu atoms form a hexagonal net, two phosphorus atoms are situated above and below the centers of the hexagon, respectively. Note the exceptional similarity.

IX. SUMMARY AND CONCLUSIONS

We have determined the magnetic ordering in semimetallic EuAs₃ and the solid solutions Eu(As_{1-x}P_x)₃ by neutron diffraction on single crystals. Semimetallic EuAs₃ and Eu(As_{1-x}P_x)₃ order at T_N with second-order phase transition to a sine-wave amplitude modulated phase with the magnetic moment $\mathbf{m} \parallel [010]$ or $[0\bar{1}0]$ direction. As the temperature is lowered these compounds undergo further first-order phase transition at T_L either to a commensurate antiferromagnetic phase with $\mathbf{m} \parallel [010]$ or $[0\bar{1}0]$ for lower P concentrations or to a helimagnetic phase with magnetic moments modulated in direction and amplitude in the (010) plane for higher P concentrations. The semiconducting β -EuP₃ is on the other hand a simple antiferromagnet with a second-order phase transition at T_N and shows no temperature-induced phase transition down to $T=2$ K.

From the basis of the present investigations the following conclusions are made:

(1) The magnetic properties of the semiconductor β -EuP₃ are very simple and are what one expects for Eu²⁺ ions in ⁸S_{7/2} state.

(2) The semimetallic EuAs₃ and Eu(As_{1-x}P_x)₃ have complex magnetic ordering for the S -state Eu²⁺ ions. However, by assuming anisotropic exchange interaction the stabilities of the incommensurate and the commensurate phases of EuAs₃ can be phenomenologically understood.

(3) The temperature variation of the modulation vector of the incommensurate phase of EuAs₃ follows the predictions of the sine-Gordon soliton-lattice theory. Nevertheless, there are some problems with the soliton-lattice interpretation of the incommensurate phase of EuAs₃. The lock-in transition is not really continuous but is ultimately of first order. The temperature variation of the modulation vector predicted by the soliton-lattice model is, in principle, continuous, but the logarithmic variation of the modulation vector for $T \rightarrow T_L$ is virtually indistinguishable from a discontinuous first-order lock-in transition.

(4) If the temperature decreases appreciably below T_N , secondary satellites due to higher harmonics of the distorted phase should, in principle, appear in the soliton-lattice model. However, these higher-order satellites have not been observed possibly due to their very low intensities.

(5) The soliton-lattice behavior of the temperature variation of the wave vector is no longer observed in Eu(As_{1-x}P_x)₃ with $x=0.40$. Instead a linear variation of the wave vector is observed. This behavior is consistent with the theory due to Bruce *et al.*¹⁴ However, the reason for this crossover from soliton-lattice to linear behavior for higher P concentrations is not understood.

(6) The magnetic ordering of Eu(As_{1-x}P_x)₃ for $x=0.98$ is significantly different from those of lower x . For $x=0.98$ the sine-wave modulated phase undergoes a first-order transition to a helimagnetic phase in which the moments are modulated in the (010) plane. This sine wave to helimagnetic transition has been predicted for

the weak-anisotropy case but has been experimentally observed for the first time in $\text{Eu}(\text{As}_{1-x}\text{P}_x)_3$ with $x=0.98$. However, it is not clear why this sine wave to helimagnetic transition is favored for large P concentrations.

(7) As a final conclusion we add that the semimetallic EuAs_3 and the solid solutions $\text{Eu}(\text{As}_{1-x}\text{P}_x)_3$ show magnetic behavior which is as exciting as the Ce mononpnictides. The origin of the anisotropy is not understood at the present state of knowledge. However, the proximity of Eu 4*f* state to the Fermi level in the semimetallic EuAs_3 might lead to the *p-f* hybridization giving rise to anisotropy. More theoretical investigations to understand the magnetic properties of EuAs_3 and $\text{Eu}(\text{As}_{1-x}\text{P}_x)_3$ are urgently needed.

ACKNOWLEDGMENTS

We wish to thank Dr. J. Rossat-Mignod for critical discussions, Dr. M. Wittmann and Dr. E. Schönerr for the crystals, and Mr. E. Kisela for their orientation and cutting. The experiments have been performed at the Institut-Langevin and the financial support of this Institute is gratefully acknowledged. One of us (T.C.) wishes to thank Sonderforschungsbereich-125 Köln-Jülich-Aachen for the financial support.

$$\begin{aligned} \mathbf{M}(\mathbf{k}) &= \int \mathbf{M}(\mathbf{r}) e^{i\mathbf{k}\cdot\mathbf{r}} d\mathbf{r} \\ &= \sum_l \sum_i \sum_j f_i(\mathbf{k}) e^{i\mathbf{k}\cdot(\mathbf{r}_l + \tilde{\mathbf{R}}_j \mathbf{r}_i + \mathbf{t}_j)} \tilde{\mathbf{T}}_j \mathbf{R}_j \frac{1}{2} [(\mathbf{S}_{iu} - i\mathbf{S}_{iv}) e^{i(\tau \cdot \mathbf{r}_l + \phi_{ij})} + (\mathbf{S}_{iu} + i\mathbf{S}_{iv}) e^{-i(\tau \cdot \mathbf{r}_l + \phi_{ij})}] , \end{aligned} \quad (\text{A2})$$

where $f_i(\mathbf{k}) = \int \rho_i(r) e^{i\mathbf{k}\cdot\mathbf{r}} d\mathbf{r}$ is the form factor of the *i*th atom.

There are two simple ways of defining the relative phases ϕ_{ij} . They may all be zero, in which case the phase of the modulation for all atoms within a single unit cell is the same. Alternatively, ϕ_{ij} may be given by $\tau \cdot (\tilde{\mathbf{R}}_j \mathbf{r}_i + \mathbf{t}_j)$ in which case the phase varies smoothly throughout the structure. For the first case ($\phi_{ij}=0$) the magnetic structure factor simplifies to

$$\begin{aligned} \mathbf{M}(\mathbf{k}) &= [\mathbf{F}_u(\mathbf{k}) - i\mathbf{F}_v(\mathbf{k})] \delta(\mathbf{k} + \boldsymbol{\tau} - \mathbf{g}) \\ &\quad + [\mathbf{F}_u(\mathbf{k}) + i\mathbf{F}_v(\mathbf{k})] \delta(\mathbf{k} - \boldsymbol{\tau} - \mathbf{g}) , \end{aligned} \quad (\text{A3})$$

where \mathbf{g} is a reciprocal-lattice vector and

$$\mathbf{F}_u(\mathbf{q}) = \sum_i \sum_j f_i(\mathbf{k}) \tilde{\mathbf{T}}_j \tilde{\mathbf{R}}_j \mathbf{S}_{iu} e^{i\mathbf{q}\cdot(\tilde{\mathbf{R}}_j \mathbf{r}_i + \mathbf{t}_j)}$$

is the unit-cell structure factor corresponding to one component of the modulation; $\mathbf{F}_v(\mathbf{q})$, defined similarly, corresponds to the other. In the case where the phase of the modulation varies smoothly,

APPENDIX A

A sinusoidally modulated antiferromagnetic structure may be described by a magnetization density:

$$\begin{aligned} \mathbf{M}(\mathbf{r}) &= \sum_l \sum_i \sum_j \rho_i(\mathbf{r} - \mathbf{r}_l - \tilde{\mathbf{R}}_j \mathbf{r}_i - \mathbf{t}_j) \tilde{\mathbf{T}}_j \cdot \tilde{\mathbf{R}}_j \\ &\quad \times [\mathbf{S}_{iu} \cos(\mathbf{r}_l \cdot \boldsymbol{\tau} + \phi_{ij}) \\ &\quad \quad + \mathbf{S}_{iv} \sin(\mathbf{r}_l \cdot \boldsymbol{\tau} + \phi_{ij})] , \end{aligned} \quad (\text{A1})$$

where $\boldsymbol{\tau}$ is the propagation vector of the magnetic structure, \mathbf{r}_l is a lattice vector, \mathbf{r}_i gives the position in the unit cell of the *i*th atom, $\tilde{\mathbf{R}}_j$ is the rotation and \mathbf{t}_j the translation associated with the *j*th symmetry operator of the space group, $\tilde{\mathbf{T}}_j$ is the magnetic operator associated with the *j*th symmetry operator (it is either the identity operator or the time-reversal operator), \mathbf{S}_{iu} and \mathbf{S}_{iv} are two mutually perpendicular vectors which describe the magnitude and direction of the spin on the *i*th atom, ϕ_{ij} , is the phase of the modulation at $\tilde{\mathbf{R}}_j \mathbf{r}_i + \mathbf{t}_j$, and $\rho_i(r)$ is a scalar magnetization density associated with the *i*th atom which for simplicity will be assumed spherically symmetric. The summations are over the lattice vectors *l*, the different magnetic atoms in the cell *i*, and the elements of the space group *j*.

The magnetic structure factor corresponding to this density is

$$\begin{aligned} \mathbf{M}(\mathbf{k}) &= [\mathbf{F}(\mathbf{g}) - i\mathbf{F}_v(\mathbf{g})] \delta(\mathbf{k} + \boldsymbol{\tau} - \mathbf{g}) \\ &\quad + [\mathbf{F}(\mathbf{g}) + i\mathbf{F}_v(\mathbf{g})] \delta(\mathbf{k} - \boldsymbol{\tau} - \mathbf{g}) . \end{aligned} \quad (\text{A4})$$

In all cases the magnetic intensity is proportional to

$$|[\mathbf{k} \times \mathbf{M}(\mathbf{k}) \times \mathbf{k}] / \mathbf{k}^2|^2 .$$

For the monoclinic structure of EuAs_3 and EuP_3 , in which the europium atoms lie in mirror planes, there are two possibilities compatible with the symmetry: either \mathbf{S}_u is parallel to [010] and $\mathbf{S}_v=0$, giving an amplitude modulated structure, or both \mathbf{S}_u and \mathbf{S}_v lie in the (010) plane, which gives a spiral spin structure possibly with an elliptical envelope. For the [010] moment the magnetic space group is one in which the mirror plane is not combined with spin reversal, whereas for moments in the (010) phase it is. Thus these two models should be independent if the mirror plane remains an element of the magnetic space group.

APPENDIX B

Patterson¹⁷ in 1934 showed that the Fourier transformation of the intensities of Bragg reflections of rays

from a crystal gives the autocorrelation function $P(\mathbf{u})$ of the electron density distribution,

$$P(\mathbf{u}) = \int \rho(\mathbf{r})\rho(\mathbf{u}-\mathbf{r})d\mathbf{r}, \quad (\text{B1})$$

where $\rho(\mathbf{r})$ is the electron density. The function $P(\mathbf{u})$ has maxima of weight $\rho_m\rho_n$ at vector distances $\gamma_m - \gamma_n$ from the origin where γ_m and γ_n are the position vectors of atoms of atomic numbers ρ_m and ρ_n , respectively. In a similar way a magnetic correlation function $Q(\mathbf{u})$ may be defined as a scalar-product autocorrelation function for the magnetization density distribution $\mathbf{M}(\mathbf{q})$ such that

$$\begin{aligned} Q(\mathbf{u}) &= \sum_{\mathbf{q}} |\mathbf{M}(\mathbf{q})|^2 e^{i\mathbf{q}\cdot\mathbf{u}} \\ &= \sum_{\mathbf{g}} \sum_n |\mathbf{M}(\mathbf{g}-n\mathbf{k})|^2 \exp[i(\mathbf{g}-n\mathbf{k})\cdot\mathbf{u}], \end{aligned} \quad (\text{B2})$$

where $\mathbf{q} = \mathbf{g} - n\mathbf{k}$, \mathbf{q} is the scattering vector, \mathbf{g} is the

reciprocal-lattice vector, \mathbf{k} is the propagation vector, and $n = \pm 1$.

It is, however, not $|\mathbf{M}(\mathbf{q})|^2$ which is measured in a neutron scattering experiment but

$$\begin{aligned} I(\mathbf{q}) &\propto |[\mathbf{q} \times \mathbf{M}(\mathbf{q}) \times \mathbf{q}] / q^2|^2 \\ &= |\mathbf{M}(\mathbf{q})|^2 - |\mathbf{q} \cdot \mathbf{M}(\mathbf{q})|^2 / q^2, \end{aligned} \quad (\text{B3})$$

and it is the second term, dependent upon the relative orientation of the magnetic structure factor and the scattering vector \mathbf{q} , that allows determination of the moment direction. The Fourier transform of $I(\mathbf{q})$ is the spin-density Patterson function and can be written as the difference of two terms: $Q(\mathbf{u})$ discussed above, and $R(\mathbf{u})$ being the Fourier transform of the second term. The interpretation of $R(\mathbf{u})$, has been discussed by Wilkinson.^{18,19} In general it gives peaks at the same positions as those of $Q(\mathbf{u})$ but these peaks, rather than being spherical, are elongated along a direction bisecting the angle between the two moments giving rise to the peak.

¹W. Bauhofer, M. Wittmann, and H. G. v. Schnering, *J. Phys. Chem. Solids* **42**, 687 (1984).

²M. Möllendorf, Ph. D. thesis, University of Stuttgart, 1984.

³W. Bauhofer, E. Gmelin, M. Möllendorf, R. Nesper, and H. G. v. Schnering, *J. Phys. C* **1**, 3017 (1985).

⁴T. Chattopadhyay, H. G. v. Schnering, and P. J. Brown, *J. Magn. Magn. Mater.* **28**, 247 (1982).

⁵T. Chattopadhyay, P. J. Brown, P. Thalmeier, and H. G. v. Schnering, *Phys. Rev. Lett.* **57**, 372 (1986).

⁶W. Bauhofer, T. Chattopadhyay, M. Möllendorf, E. Gmelin, H. G. v. Schnering, U. Steigenberger, and P. J. Brown, *J. Magn. Magn. Mater.* **54-57**, 1359 (1986).

⁷T. Chattopadhyay, H. Bartholin, J. Voiron, W. Bauhofer, and H. G. v. Schnering, *J. Magn. Magn. Mater.* **63&64**, 632 (1987).

⁸M. Wittmann, W. Schmettow, D. Sommer, W. Bauhofer, and H. G. v. Schnering, in *Proceedings of the 6th International Conference on Solid Compounds of Transition Elements* (Stuttgart, 1979) (unpublished).

⁹L. Koester in *Neutron Physics*, Vol. 80 of *Springer Tracts in Modern Physics*, edited by G. Höhler (Springer-Verlag, Berlin, 1977), p. 1.

¹⁰A. J. Freeman and J. P. Desclaux, *J. Magn. Magn. Mater.* **12**, 11 (1979).

¹¹E. Gmelin *et al.* (unpublished).

¹²P. J. Brown, *Physica* **137B**, 31 (1986).

¹³P. Bak and J. Boehm, *Phys. Rev. B* **21**, 5297 (1980); W. L. McMillan, *ibid.* **14**, 1496 (1976).

¹⁴A. D. Bruce, R. A. Cowley, and A. F. Murray, *J. Phys. C* **11**, 3591 (1978).

¹⁵T. Chattopadhyay and P. J. Brown, *Phys. Rev. B* **36**, 2454 (1987).

¹⁶J. Rossat-Mignod, in *Neutron Scattering in Condensed Matter*, edited by K. Sköld and D. L. Price (Academic, New York, 1986).

¹⁷A. L. Patterson, *Phys. Rev.* **46**, 368 (1934).

¹⁸C. Wilkinson, *Philos. Mag.* **17**, 609 (1968).

¹⁹C. Wilkinson, *Acta Crystallogr. Sect. A* **29**, 449 (1973).